Applied Surface Science 387 (2016) 419–430

Contents lists available at ScienceDirect

Applied Surface Science

journal homepage: www.elsevier.com/locate/apsusc

Preparation and characterization of zirconia-loaded lignocellulosic butanol residue as a biosorbent for phosphate removal from aqueous solution

Enmin Zong[a], Xiaohuan Liu[b,*], Jinhua Jiang[a], Shenyuan Fu[b], Fuxiang Chu[c]

[a] Zhejiang Provincial Key Laboratory of Plant Evolutionary Ecology and Conservation, Taizhou University, Taizhou 318000, PR China
[b] School of Engineering, National Engineering and Technology Research Center of Wood-Based Resources Comprehensive Utilization, and Key Laboratory of Wood Science and Technology of Zhejiang Province, Zhejiang Agriculture and Forestry University, Hangzhou, Lin'an 311300, PR China
[c] Institute of Chemical Industry of Forestry Products, CAF, Nanjing 210037, PR China

ARTICLE INFO

Article history:
Received 26 March 2016
Received in revised form 11 June 2016
Accepted 18 June 2016
Available online 21 June 2016

Keywords:
Lignocellulosic butanol residue
Zirconium
Biosorbent
Phosphate removal
Adsorption isotherms
Mechanism

ABSTRACT

Zirconium(IV) loaded lignocellulosic butanol residue (LBR-Zr) used for the adsorption of phosphate (P) ions from aqueous solution was synthesized and evaluated. The adsorption isotherms were fitted well with the Freundlich and Temkin modes. Thermodynamic analyses indicated that phosphate adsorption on the LBR-Zr increased with increasing temperature from 298 to 338 K. The kinetic datas were described better by the pseudo-second-order adsorption kinetic rate model. Increasing pH suppressed phosphate adsorption. Coexisting anions study exhibited that the incorporation of CO_3^{2-} anion had the largest influence on the phosphate adsorption capacity. The mechanism of adsorption process on LBR-Zr was analyzed by FTIR (Fourier transform infrared spectroscopy), scanning electron microscope (SEM) with an EDX (energy dispersive X-ray) and X-ray photoelectron spectroscopy (XPS) technologies, respectively. The above results confirmed that surface hydroxyl groups on biosorbent LBR-Zr were replaced by phosphate. The LBR-Zr with good specific affinity towards phosphate was a promising biosorbent for phosphate removal from aqueous solution. The research would be beneficial for developing a promising, eco-friendly phosphate biosorbent from plentiful lignocellulosic butanol residue.

1. Introduction

Phosphorus (P) is a very important limiting nutrient for growth of organisms [1]. It plays a major role in the development of animals, plants and the industrial manufacture [2]. However, the extensively application of phosphate has caused serious environmental issues. Particularly, the residue of phosphates in water with a large amount may cause eutrophication leading to excessive growth of algal called algal blooms [3]. Furthermore, it is recommended that a criterion maximum contaminant level for phosphate ions is less than 0.05 mg L^{-1} by the United States Environmental Protection Agency (USEPA) [4]. As a consequence, it is necessary to develop certain efficient methods to remove phosphate ions from water. Presently, the methods used for the removal of phosphate from water were summarized as chemical precipitation, ion exchange, crystallization, biological treatment, and adsorption methods [1,5–9]. Among these methods, the adsorption method is usually considered to be superior to other techniques when being applied in the remove of pollutants from aqueous solutions because of its simpleness, effectivity, and low cost [10]. There has been growing interest in developing novel, low-cost and sustainable biosorbents for phosphate removal using renewable agricultural by-products such as apple peels [11], okara [12], soybean milk [13], aspen wood fiber [14], eggshell [15], wood particles [16], coir pith [17], orange waste gel [1].

The lignocellulosic butanol residue is a byproduct obtained from industrial of bio-butanol, a superior liquid fuel with a potential to substitute for fossil fuel. The bio-butanol was produced by the method of biorefinery processes based on agricultural biomass such as wheat straw and corn, and meanwhile, and generated a larger quantity of lignocellulosic butanol residue (LBR) as a by-product [18]. As expected, the further uitilzation of LBR therefore can reduce the cost of production of bio-butanol [19]. Lignin is the main component of LBR, in which the content of lignin is higher than eighty percent. It was acknowledged that lignin exhibited high capture abilities to various heavy metals [20–23]. To the best of our

* Corresponding author.
E-mail address: liuxiaohuancaf@163.com (X. Liu).

http://dx.doi.org/10.1016/j.apsusc.2016.06.107
0169-4332/

Table 1
Composition and functional group content of LBR (wt.%).[a]

Sample	Ash	Lignin	Holocellulose	Polysaccharide	Total hydroxyl	Phenolic hydroxyl	Aliphatic hydroxyl	Methoxyl
LBR	3.9	81.0	11.9	1.5	20.9	3.3	17.6	2.7

[a] The data was from Zhang et al. [18].

knowledge, it has not been reported the utilization of LBR for removal phosphate.

Generally, cationic binding sites were usually introduced into sorbent by metal impregnation to improve their uptake capacity of phosphate. As a consequence, cationization of agricultural by-product is widely used for activating its phosphate sorption ability using metal salts. Many studies have been reported, which confirm the enhanced phosphate removal of metals loaded biosorbents [2,12,16,24].

For LBR, apart from the function groups (e.g. −OH) derived from lignin, it also reported to have −CHO and −COOH, which allows LBR to be facilely chemical modification. For example, the introduction of alkoxyamine ligands can afford LBR with anion exchange abilities. Therefore, these unique properties of LBR enable LBR to be a promising substrate for developing phosphate biosorbents [25–29].

During the last decades, several different metallic oxides including Fe(III), La(III), Zn(IV), and Ce(III) oxides used as cationic binding site, have been developed as phosphate adsorbents [14,17,30,31]. Among of these metal oxides, hydrous Zr(IV) oxide has been receiving lots of in eliminating phosphate because of its high binding affinity for phosphate and high physicochemical stability over the whole pH range [32]. Furtherly, our previous studies also demonstrated that incorporating hydrous zirconium could dramatically improve phosphate sorption abilities of nano-paricles [32,33].

Herein, in this context, we immobilized zirconium oxide (ZrO_2) to LBR by post-grafting method, which can be used as a novel biosorbent (LBR-Zr) for removing phosphate ions from water. To the best of our knowledge, our research is the first report to load zirconium on LBR as adsorbent for phosphate removal from aqueous solution.

In this work, the feasibility of using ZrO_2-loading LBR biosorbent (LBR-Zr) as an adsorbent for phosphate removal from aqueous solutions was evaluated in batch experiments. The absorption isotherms, kinetics involved in the adsorption process were discussed. Meanwhile, several factors affecting the phosphate adsorption such as pH value, initiate phosphate concentration, temperature and the incorporation of foreign anions were also investigated. In addition, the underlying mechanism for phosphate adsorption was fully studied by SEM-EDX, FTIR and XPS technologies. This study could provide a new pathway for phosphate adsorption based on by-products of the bio-butanol industries (lignocellulosic butanol residue).

2. Materials and methods

2.1. Materials

The lignocellulosic butanol residue (LBR) used in the present study was a byproduct of a biobutanol industrials supplied by songyuan bairui bio-polyos Co., Ltd. (China) and used without further purification. The LBR mainly contained 81.0 wt.% lignin, 11.9 wt.% Holocellulose, 3.9 wt.% Ash and so on [18], and the results are shown in Table 1. Zirconium isopropoxide ($Zr(OC_3H_7)_4$) solution in propanol was purchased from Aldrich Chemical Co., Ltd. and used as received without further purification. All the other chemical reagents such as KH_2PO_4, KCl, KNO_3, K_2SO_4, $KHCO_3$, K_2CO_3, NaF, NaOH and HCl were of analytical grade and used as obtained.

2.2. Preparation of lignocellulosic butanol residue loading Zr(IV) (LBR-Zr)

The reaction was carried out in a dry 50 mL schlenk flask equipped with a magnetic stirrer. A 1.0 g of LBR was dissolved in 20 mL DMSO with stirring until the reaction mixture became homogeneous. The schlenk flask was immersed in a silicone oil bath set at 110 °C. 1.5 mL of 70% zirconium isopropoxide ($Zr(OC_3H_7)_4$) solution in propanol was gradually added into the above mixture and the reaction was run for 3 h with stirring. The resulting product was finally precipitated with *n*-hexane, collected and washed successively by anhydrous ethanol and deionized water in sequence. The precipitation was dried under vacuum until a constant weight was reached, and the resulting material was denoted as LBR-Zr. The obtained LBR-Zr was stored in a desiccator for further use.

2.3. Adsorption studies

The adsorption experiments were conducted in batch method at 298 K. Appropriate amount of anhydrous KH_2PO_4 was dissolved in distilled water as a phosphate ion stock solution (1000 mg P L^{-1}) and then further diluted to desired concentration. Each experiment was conducted at the pH of the stock solution (6.0 ± 0.2), which was adjusted to desired value with 0.1 mol L^{-1} HCl or 0.1 mol L^{-1} NaOH solution. At the end of adsorption process, all samples containing phosphate were filtered through a 0.45-μm membrane filter and then the concentrations of phosphate ions were determined by molybdate blue spectrophotometric method. All the sorption experiments were performed in duplicate, and the experimental details were given in the related figures and tables. The equilibrium sorption capacity was calculated from:

$$q_e = \frac{(C_0 - C_e)V}{m} \quad (1)$$

where q_e (mg g^{-1}) is the equilibrium adsorption amount, C_0 (mg L^{-1}) is the initial phosphate concentration, C_e (mg L^{-1}) is the equilibrium concentration, V (mL) is the solution volume, and m (g) is the adsorbent mass.

The adsorption kinetic experiments for LBR-Zr were carried out at 298 K, and initial concentrations were 5, 10 and 20 mg P L^{-1} with pH 6.0 ± 0.2 respectively. After a specific time interval, about 1.0–2.0 mL aliquots were withdrawn from the suspensions for the analysis of phosphate concentrations. The study of the pH (2–8) dependency of phosphate onto LBR-Zr was carried out with 40 mg L^{-1} initial phosphate concentration at 298 K. The effect of temperature was studied by using 20 mg L^{-1} initial phosphate concentration at three temperatures (298, 318 and 338 K). The effect of foreign anions (Cl^-, NO_3^-, F^-, SO_4^{2-}, CO_3^{2-} and HCO_3^-) with concentrations of 300 mg L^{-1} separately was also investigated at 298 K under a fixed initial concentration of 40 mg L^{-1} phosphate solutions, and initial solution pH of 6.0 ± 0.2.

2.4. Adsorbent characterization

2.4.1. X-ray photoelectron spectroscopy (XPS) analysis

The chemical composition of LBR, LBR-Zr and LBR-Zr-P (after phosphate adsorption) samples were carried out to investigate using a PHI 5000 Versa Probe XPS spectrometer (ESCALAB 250 US Thermo Electron Co.), and the experimental data were fitted with

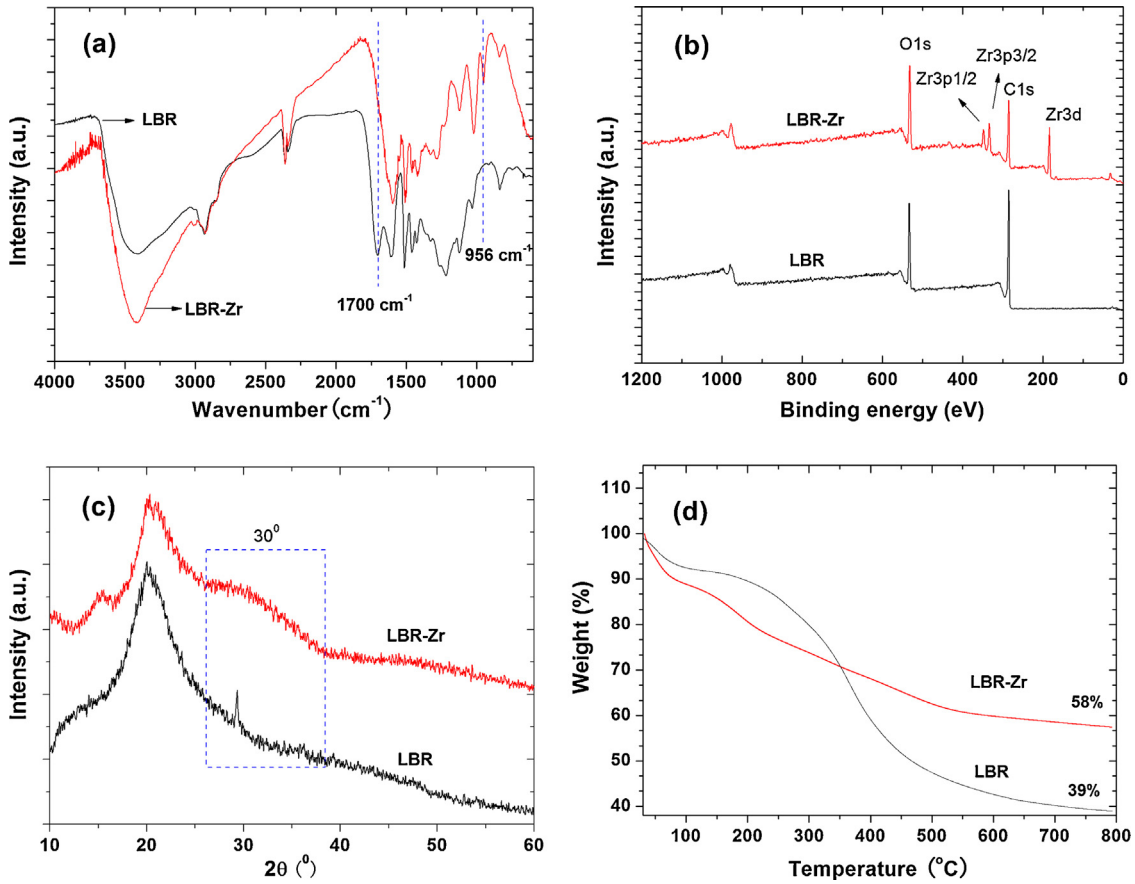

Fig. 1. FTIR (a) and XPS (b), XRD (c) and TGA (d) spectra of LBR and LBR-Zr, respectively.

Table 2
Structure properties of the absorbent.

Sample	Appearance	ZrO_2 content[a](%)	S_{BET} ($m^2\,g^{-1}$)	V_p ($cm^3\,g^{-1}$)
LBR	Dark brown powder	–	16.38	0.042
LBR-Zr	Black powder	6.969[a]	76.38	0.167

[a] Determined by XPS.

XPSPEAK41 and Origin 7.5 for analysis. The C1 s peak at 284.6 eV was used as a standard for the calibration of binding energy value. The characteristic X-rays focus on C, O, Zr and P in this study.

2.4.2. Fourier transform infrared (FTIR) analysis

The FTIR spectra of LBR, LBR-Zr and LBR-Zr-P (after phosphate adsorption) samples are recorded using a Model Perkin Elmer 1100 series operating in the region of 4000–400 cm $^{-1}$ using KBr pellet technique.

2.4.3. X-ray diffractomer (XRD) analysis

XRD spectra of the LBR and LBR-Zr samples were obtained from a Rigaku D/max-RA power diffraction-meter using Cu Kα radiation in the 2θ range of 10–60° at 5° min^{-1}.

2.4.4. Scanning electron microscopy (SEM) examination with energy-dispersive-X-ray spectroscopy (EDX) analysis

The surface morphology of LBR, LBR-Zr and LBR-Zr-P (after phosphate adsorption) samples were performed to investigate using a Hitachi S-4800 field emission scanning electron microscope (SEM) with a Bruker Energy Dispersive X-ray spectroscopy (EDX) detector. Prior to testing for SEM, each sample was sputter-coated with gold.

2.4.5. Thermogravimetric analysis (TGA)

TGA curves of the LBR and LBR-Zr samples were recorded on a TA SDT Q600 apparatus ranging from 30 to 800 °C with a temperature change of 10 °C min^{-1} under a nitrogen flow rate of 150 mL min^{-1}.

3. Results and discussion

3.1. The characterizations and properties of LBR

The utilization of LBR in this work was taken the "catch all" pathway to use as the raw material without purification, which was different from our previous studies of origin material BBL [25–29]. The characterization of LBR was reported by Zhang et al. [18], and the main results are shown in Table 1. The LBR mainly contained 81.0 wt.% lignin, 11.9 wt.% holocellulose, 3.9 wt.% ash and so on, and showed a high hydroxyl content of 20.9 wt.% (including 3.3 wt.% phenolic-hydroxyl and 17.6 wt.% aliphatic-hydroxyl). These data constituted a key point in this work because the surface of hydroxyl groups in LBR would be functionalized [34].

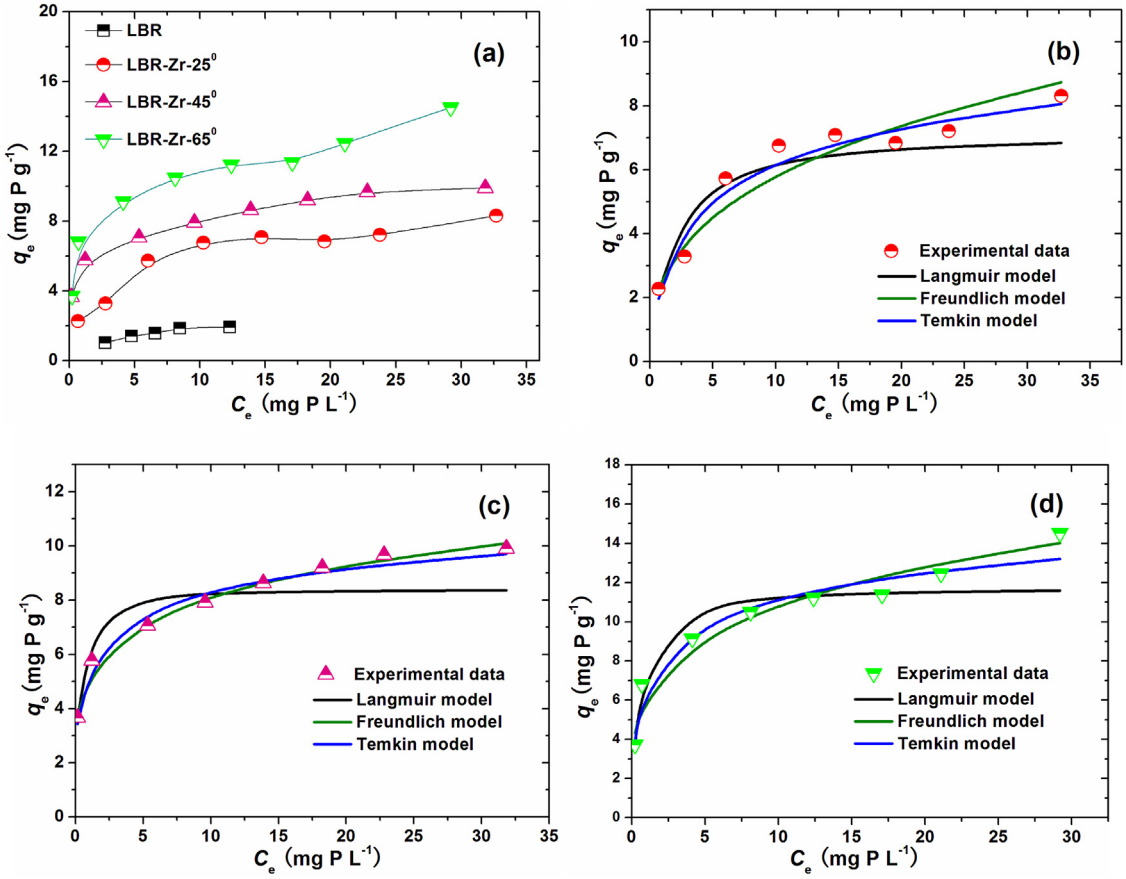

Fig. 2. Phosphate adsorption isotherms of LBR-Zr at 25 °C, 45 °C and 65 °C and LBR at 25 °C (a) and the equilibrium constants and isotherm parameters obtained from experimental data nonlinear fitting for LBR-Zr at 25 °C (b), at 45 °C (c) and at 65 °C (d). (Adsorption conditions: adsorbent dosage = 0.625 g L^{-1}, pH = 6.0 ± 0.2, equilibrium time = 48 h.)

Table 3
Adsorption equilibrium constants obtained from Langmuir, Freundlich and Temkin isotherms in the adsorption of Phosphate onto LBR-Zr.

	Temperature (K)	Langmuir isotherm constans			Freundlich isotherm constans			Temkin isotherm constants		
		b (L mg^{-1})	Qm (mg g^{-1})	R^2	K_F	n	R^2	A	B	R^2
LBR-Zr	298	0.64	7.17	0.8995	2.6414	2.91	0.9442	2.5673	1.5766	0.9445
	318	4.51	8.42	0.9054	5.2688	5.32	0.9932	5.5705	1.1941	0.9800
	338	2.13	11.78	0.9790	6.2336	4.16	0.9510	6.8135	1.8921	0.9599

3.2. Structure characterization analysis of LBR-Zr

Some physiochemical properties of LBR-Zr are presented in Table 2. The resulting adsorbent LBR-Zr was present as black powder. The specific surface areas determined on the basis of the BET results were 16.38 m^2 g^{-1} and 76.38 m^2 g^{-1} for LBR and LBR-Zr, respectively, indicating an increased surface area with ZrO_2 functionalization. The total pore volume of LBR-Zr increased from 0.042 cm^3 g^{-1} to 0.167 cm^3 g^{-1} compared to LBR, reflecting that pores had taken shape on the surface of LBR. The loading content of ZrO_2 was 6.96% in mass. The immobilization of zirconium onto LBR surface can be verified by using various techniques as followed, including FTIR, XPS, XRD, and TGA.

FTIR spectra of LBR and the LBR-Zr are presented in Fig. 1a. In the spectrum of LBR, the absorption peaks at 1651, 1500 and 1410 cm^{-1} were associated with the vibration of aromatic in lignin. It was found that a new band peak at 956 cm^{-1} was appeared in the spectrum of LBR-Zr, which confirmed the incorporation of zirconium(IV) into the lattice framework [35,36]. Meanwhile, it was worth noting that the peak at 1700 cm^{-1} attributed to the carbonyl groups of LBR disappeared when zirconium(IV) loading LBR, likely because that the carbonyl groups of LBR were coordinate with zirconium(IV) to form a chelate [37], which was in good consistence with our pervious study [32]. The results signified that zirconium(IV) was successfully loaded onto LBR.

To further illustrate the covalent functionalization, the X-ray photoelectron spectroscopy (XPS) was performed on LBR and LBR-Zr samples. The survey XPS spectra of the samples are presented in Fig. 1b. It was found that LBR-Zr exhibited Zr3d and Zr3p peaks in addition to C1s and O1s peaks, suggesting the presence of ZrO_2 on the surface of LBR, which was similar to the reported values in the literature [38].

The X-ray diffraction curves of LBR and LBR-Zr are shown in Fig. 1c. It was worth noting that a new wide diffraction peak appeared around 30° [39,40] was visible in addition to the diffraction peaks of LBR, due to the deposition of amorphous ZrO_2 on the LBR surface. It should be pointed out that the sorption of phosphate maybe mainly derived from the amorphous LBR-Zr [41].

TGA curves (Fig. 1d) showed that about 16% of the total weight of LBR-Zr was due to the removal of adsorbed water. It was observed that an obvious weight loss was recorded at a temperature of 450 °C, which corresponded to the LBR. When the temperature was higher

Table 4
The phosphate adsorption capacity of LBR-Zr in comparison with various biosorbents.

Absorbent	Phosphate adsorption capacity (mg P g^{-1})	Refs.
LBR (UM)[a]	**1.92**	**This study**
Macrophyte (UM)	0.286	Wang et al. [46]
Giant reed (UM)	0.836	Xu et al. [47]
Sugarcane bagasse (UM)	1.10	Zhang et al. [48]
Okara (UM)	0.8	Nguyen et al. [12]
Date palm fibers (UM)	4.35	Riahi et al. [49]
LBR-Zr (M)[b]	**8.75**	**This study**
Fe loaded okara (M)	4.785	Nguyen et al. [12]
Fe loaded aspen wood fiber (M)	4.30	Eberhardt et al. [14]
Zn activated coir pith carbon (M)	5.10	Namasivayam and Sangeetha [17]
Iron hydroxide eggshell(M)	14.49	Mezenner and Bensmaili [15]
Zr loaded orange waste gels(M)	57	Biswas et al. [1]
Zr loaded apple peels(M)	20.35	Mallampati and Valiyaveettil [11]
Orange waste (loaded with La, Ce, Fe) (M)	13.94	Biswas et al. [31]

[a] UM: unmodified biosorbent.
[b] M: modified biosorbent.

than 600 °C, a constant weight of 58.8% was observed corresponding to ZrO_2 in the LBR-Zr. These results indicated that the lower weight loss of LBR-Zr was due to the high content of ZrO_2 which was thermally stable.

3.3. Adsorption isotherm

Adsorption isotherm studies were conducted to determine the feasibility of an adsorption treatment. Some well-known mathematical descriptions that has been used to fit to the experimental data and assess the isotherm performance, which included the Freundlich, Langmuir, Temkin, Redlich-Paterson and Sips sorption isotherms [42]. In this study, Freundlich, Langmuir, and Temkin models were chosen to determine the adsorption equilibrium between the adsorbent and phosphate ions.

The Langmuir adsorption isotherm was suitable for one molecular layer adsorption onto the surface of adsorbent. This isotherm equation was expressed as below [43], with q_e as the amount adsorbed at equilibrium (mg g^{-1}), C_e as the equilibrium solution concentration (mg L^{-1}), b as the Langmuir adsorption model (L mg^{-1}), and Q_0 as the maximum adsorption capacity (mg g^{-1}).

$$q_e = \frac{Q_0 b C_e}{1 + bC_e} \quad (2)$$

Freundlich model was usually applicable to describe the models of multilayer absorption onto a heterogeneous surface. The Freundlich isotherm was given below as following [44]. Where K_F and n are the Freundlich constants. K_F and n are indicators of adsorption capacity and adsorption intensity, respectively.

$$q_e = K_F C_e^{1/n} \quad (3)$$

The Temkin model has been developed to describe the chemisorption, which can be expressed as following [45]. Where A and B are the Temkin constants.

$$q_e = A + B\ln C_e \quad (4)$$

Phosphate adsorption isotherms onto LBR-Zr were conducted at 298, 318 and 338 K and pH = 6.0 ± 0.2 (Fig. 2a). The fitted constants for the Langmuir, Freundlich and Temkin isotherm models along with regression coefficients (R^2) were complied in Table 3. The R^2 achieved at 318 K for Langmuir, Freundlich, Temkin models were 0.9054, 0.9932, and 0.9800, respectively (Fig. 2c). Results showed that phosphate adsorption to LBR-Zr could be both well described by Freundlich and Temkin modes compared with Langmuir mode judged from the correlation coefficients, suggesting the adsorption process occurred heterogeneously through chemical interactions [30]. It was also clearly seen that LBR-Zr had significantly high uptake capacity for phosphate (8.75 mg P g^{-1}), while pure LBR without loading zirconium exhibited negligible phosphate adsorption (1.92 mg P g^{-1}) under the same condition. LBR-Zr was 4.56 times efficient as raw LBR in eliminating phosphate. This confirmed that loading of zirconium was an efficient method in enhancing the phosphate sequestering ability of LBR.

Table 5
Thermodynamic parameters estimated for the phosphate adsorption on LBR-Zr at different temperatures (298, 318 and 338 K).

Temperature (K)	Thermodynamic parameters		
	ΔG° (kJ mol^{-1})	ΔH° (kJ mol^{-1})	ΔS° (kJ mol^{-1} K^{-1})
298	−3.268	49.658	0.178
318	−6.820	49.658	0.178
338	−10.372	49.658	0.178

As shown in Table 4, the phosphate adsorption capacity of the unmodified LBR at 1.92 mg P g^{-1} of biosorbent was high compared to some unmodified biosorbent in the literatures: e.g. 0.286 mg P g^{-1} for macrophyte, 0.836 mg P g^{-1} for giant reed, 1.10 mg P g^{-1} for sugarcane bagasse, 0.8 mg P g^{-1} for okara; the phosphate adsorption capacity of the LBR-Zr (modified) at 8.75 mg P g^{-1} is high compared to some modified biosorbent: e.g. 4.785 mg P g^{-1} for Fe loaded aspen wood fiber, 4.30 mg P g^{-1} for Fe loaded aspen wood fiber, 5.1 mg P g^{-1} for Zn activated coir pith carbon. But LBR-Zr was not high compared with the rest literature data. Although the biosorbent obtained from this study was the limited adsorption capacity of phosphate, the LBR was still recommended for developing biosorbent of phosphate because of its advantage of being abundant, cost-effectiveness, sustainable and environment friendly benign material [12].

3.4. Effect of temperature and adsorption thermodynamics

To investigate the effect of temperature on the adsorption capacity (q_e) of phosphate onto LBR-Zr, the experiments were carried out at 298, 318, and 338 K, respectively. The results are listed in Table 5, showing that an increase in adsorption capacity of phosphate with increasing the temperature from 298 K to 318 K revealed an endothermic process, which was similar to previous results [50,51]. The rise in uptake capacity at higher temperature was due to promoting the collision frequency between the sorbent and the solute which led to an increase the adsorption of phosphate on the surface of LBR-Zr [52]. Similar trend was seen for phosphate removal using iron hydroxide-eggshell waste [15].

To better understand whether the process of phosphate adsorption in LBR-Zr was spontaneous or not, the thermodynamics of

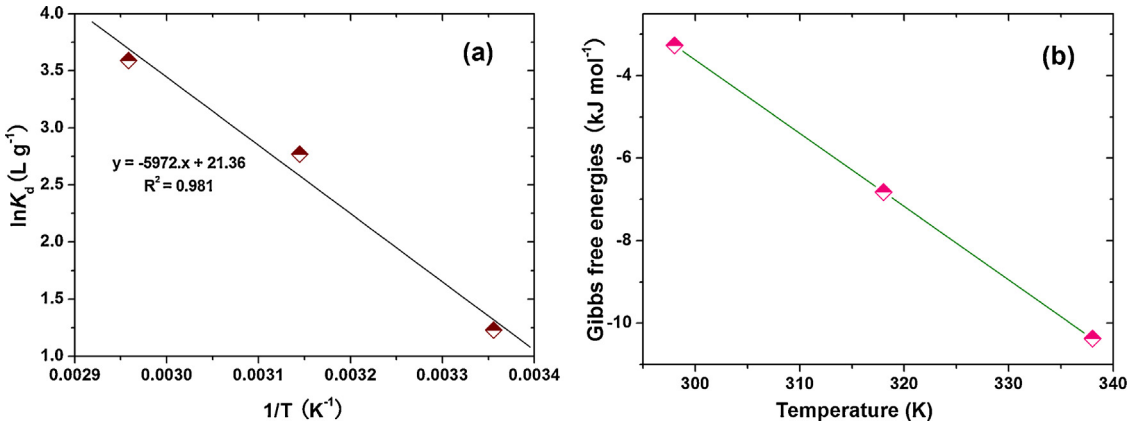

Fig. 3. The plot of $1/T$ (k^{-1}) versus $\ln k_d$ for the calculation of the thermodynamic parameters on adsorption of phosphate by LBR-Zr (a) and plot of ΔG° versus T (b).

Table 6
Comparison of kinetic parameters for the adsorption of phosphate onto the LBR-Zr with different phosphate initial concentrations (5, 10 and 20 mg P L^{-1}).

Initial concentration (mg P L^{-1})	First-order kinetic equation			Second-order kinetic equation			Experimental q_e (mg P g^{-1})
	q_e (mg P g^{-1})	k_1(min^{-1})	[a]R^2	q_e (mg P g^{-1})	k_2 (g mg^{-1} min^{-1})	[a]R^2	
5	1.98	0.0069	0.837	4.34	0.0283	0.999	4.43
10	3.84	0.0092	0.948	6.45	0.0112	0.999	6.42
20	5.05	0.0069	0.941	8.62	0.0075	0.999	8.90

[a] R^2 = coefficient of determination.

phosphate adsorption were also investigated. The thermodynamic parameters, viz., standard free energy change (ΔG°), entropy (ΔS°) and enthalpy (ΔH°) were calculated by the experimental data obtained at different temperatures (298, 318 and 338 K) using Equations (5)–(7). The equations were used as expressed in the following. Where K_d is the distribution coefficient of the adsorbent, which is computed by the ratio of the equilibrium (q_e) to equilibrium (C_e) [45,51,52]; R is the universal gas constant (8.314 J mol^{-1} K^{-1}); T is the temperature (K); the ΔS° represents the entropy (kJ mol^{-1} K^{-1}) and ΔH° denotes enthalpy (kJ mol^{-1}), respectively.

$$\Delta G^\circ = -RT\ln K_d \quad (5)$$

$$\Delta G^\circ = \Delta H^\circ - T\Delta S^\circ \quad (6)$$

$$\ln K_d = \frac{\Delta S^\circ}{R} - \frac{\Delta H^\circ}{RT} \quad (7)$$

According to Equations (5)–(7), the ΔS° and ΔH° values were determined from slope and intercept of the linear plot of $\ln k_d$ vs. $1/T$ (K^{-1}) (Fig. 3a). The plot showed good linearity with a high correlation coefficient (R^2 = 0.981). The thermodynamics parameters are presented in Table 5. The negative value of ΔG° indicated that the adsorption in this case was exergonic process. Meanwhile, the values of ΔG° decreased from −3.268 kJ mol^{-1} to −10.372 kJ mol^{-1} in the temperature range of 298–338 K (Fig. 3b), suggesting the adsorption was more efficient at a higher temperature. The value of ΔH° (49.658 kJ mol^{-1}) was positive in the process of phosphate adsorption on LBR-Zr verified that there was the endothermic nature of this adsorption reaction. The positive entropy change ΔS° value (0.178 kJ mol^{-1} K^{-1}) implied the enhanced randomness and an increased in the degrees of freedom at the solid-liquid interface during adsorption through the removal of the phosphate on the active site of the adsorbent [53].

3.5. Adsorption kinetics

The kinetic of adsorption is one of the most important factors in assessing adsorbent efficiency. A series of experiments had been carried out to study the kinetics for the absorption of phosphate by LBR-Zr. Phosphate removal by LBR-Zr as a function of contact time with different initial concentrations (5 mg P L^{-1}, 10 mg P L^{-1} and 20 mg P L^{-1}) are shown in Fig. 4a, the phosphate adsorption process with the initial concentration of 5 mg P L^{-1} was similar to that of 10 and 20 mg P L^{-1}. It was clearly seen that, a higher uptake of phosphate capacity increased with an increase in initial phosphate concentration, and a longer equilibrium time reached. The phosphate amount was found to be 4.43, 6.45 and 8.62 mg P g^{-1}, respectively, and meanwhile the reached equilibrium at about 250, 489 and 712 min, respectively.

To elucidate the absorption process, the pseudo-first-order and pseudo-second-order kinetic models were applied to fit experimental data obtained from batch experiments. The pseudo-first-order model is mathematically equivalent to a mass action rate equation for adsorption kinetics, while the pseudo-second-order model assumes that the rate-limiting step is chemisorption of phosphate ions onto adsorbent binding sites. In this study, the kinetic data were both fitted by the pseudo-first-order and pseudo-second-order models. The kinetic equations can be expressed as the following Equations (8) and (9) [54,55]. Where q_t is the adsorbed amount (mg g^{-1}) at time t (min), q_e is the adsorbed amount in equilibrium (mg g^{-1}), k_1 and k_2 are the equilibrium rate constant of pseudo-first-order model and pseudo-second-order model (g mg^{-1} min^{-1}), respectively.

Pseudo- first-order model:

$$\log(q_e - q_t) = \log q_e - \frac{k_1 t}{2.303} \quad (8)$$

Pseudo-second-order model:

$$\frac{t}{q_t} = \frac{1}{k_2 q_e^2} + \frac{t}{q_e} \quad (9)$$

The linearized forms of pseudo-first-order and pseudo-second-order models are showed in Fig. 4b and c, respectively. As shown in Fig. 4b, it was found that a significant deviation of the equilibrium adsorption amounts (q_e) obtained from fitting results from the experimental data was observed, indicating that pseudo-first-order kinetic model didn't agree with the present adsorption process.

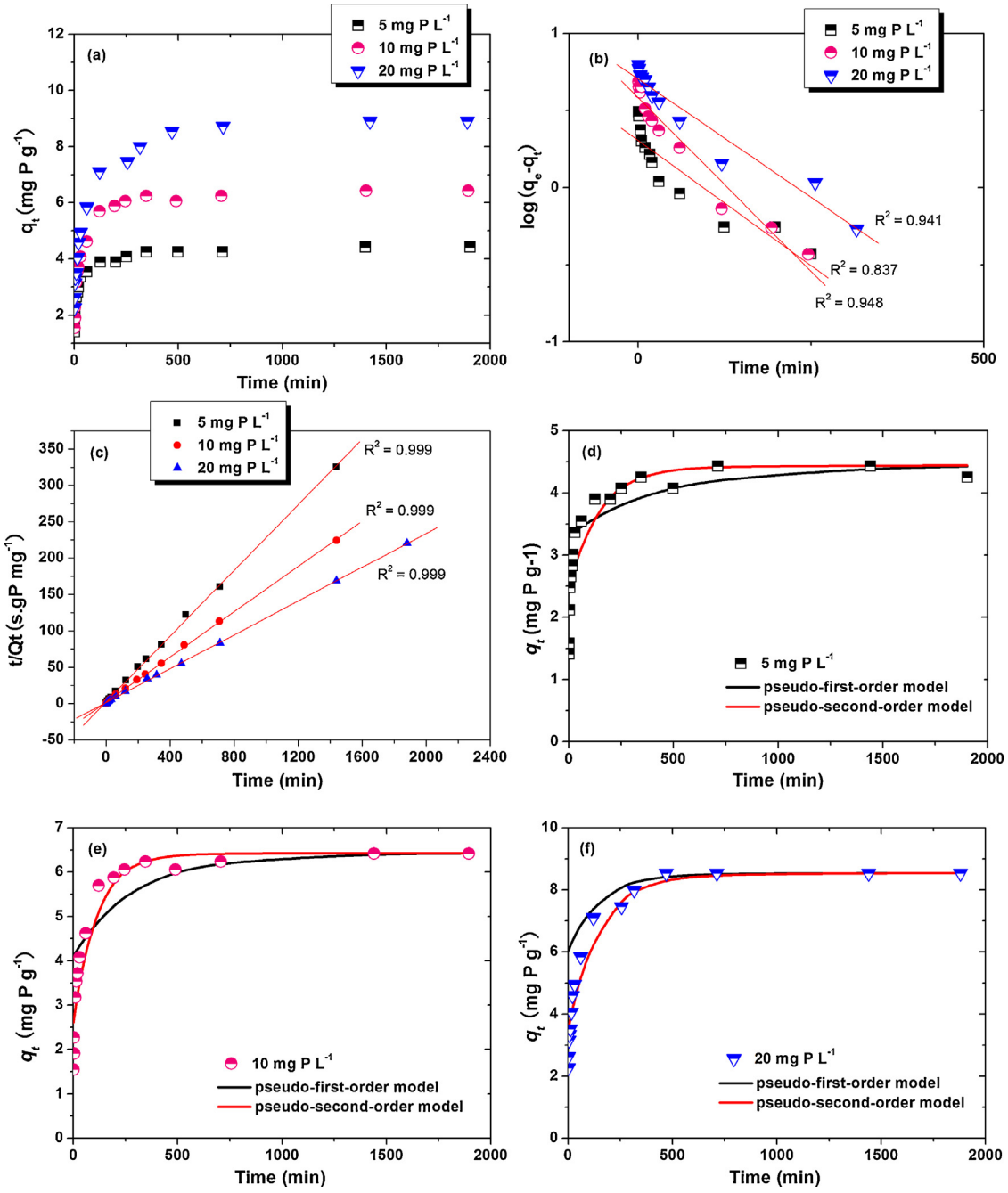

Fig. 4. Effect of contact time and initial concentration on the adsorption amount of phosphate onto LBR-Zr (a), pseudo-first-order (b) and pseudo-second-order (c) plots linear plots for the removal of phosphate at different initial concentrations, and kinetic curves of phosphate adsorption on LBR-Zr at different initial phosphate concentrations 5 mg P g^{-1} (d), 10 mg P g^{-1} (e) and 20 mg P g^{-1} (f).

On the other hand, as shown in Fig. 4c, the results were given a very good correlation with pseudo-second-order equation and linear fittings for t/q_t versus t at all concentration levels of 5, 10 and 20 mg P L^{-1}, and the regression coefficients (R^2 values) for the linear plots were all higher than 0.99 for all these studies (Fig. 4d–f). The kinetic parameters for two models are summarized in Table 6. The higher R^2 values confirmed that the absorption data were well represented by second-order model and thus supported the assumption behind the model that the sorption was due to chemisorption [54]. Besides, at initial concentrations of 5, 10 and 20 mg P L^{-1}, the rate constants (k_2) corresponding to the removal rate of phosphate were calculated to be 0.0283, 0.0112 and 0.0075 g mg^{-1} min^{-1}, respectively, which indicated the more favorable adsorption at low concentrations [32]. It was worth pointing out that the calculated q_e values obtained from fitting results were nearly close to the experimental data. The results from phosphate adsorption kinetics experiments fitted with the pseudo-second-order equation indicated a chemisorption process involving valence forces through the coordination or exchange of electrons between the adsorbent and phosphate [30,32,56,57]. Several publications about the kinetics of phosphate adsorption on adsorbents had been reported better correlations for pseudo-second order mode [10,24,58].

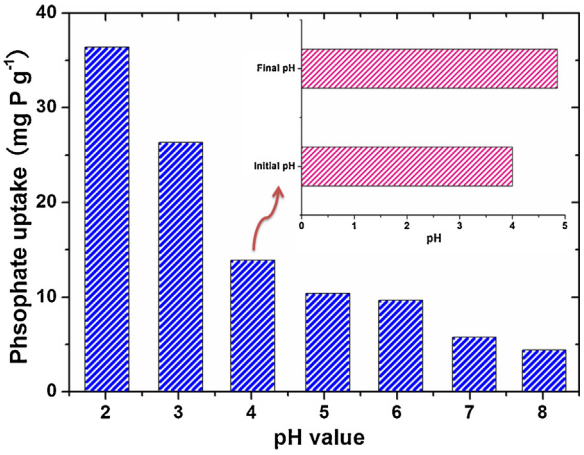

Fig. 5. Effect of initial pH value on adsorption (initial phosphate concentration: 40 mg P L^{-1}; LBR-Zr dose: 0.5 g L^{-1}; orbital shaking rate: 120; temperature: 298 K and contact time: 24 h).

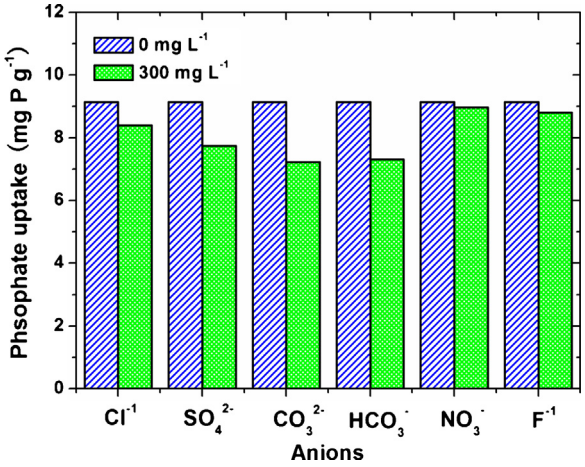

Fig. 6. Effect of foreign anions on adsorption capacity (initial phosphate concentration: 40 mg P L^{-1}; LBR-Zr dose: 0.5 g L^{-1}; orbital shaking rate: 120; temperature: 298 K and contact time: 24 h).

3.6. Effect of pH value

The effect of pH value is important for the adsorption of phosphate (P) ions solution onto the LBR-Zr since the uptake of phosphate ions on the surface of the solid particles of adsorbent is often affected by pH values [7,59]. The results are listed in Fig. 5. It was clearly seen that an increased phosphate adsorption capacity from 4.4 to 36.38 mg P g^{-1} with the solution pH decreased from 8.02 to 2.02. Evidently, the binding of phosphate anions was most efficient in acidic medium. This phenomenon was explained by the fact that at high pH values, the surface of LBR-Zr formed more negatively charged because of OH^- ions, resulting in a strong competition for the binding sites with phosphate anions. On the contrast, low pH enhanced the adsorption of phosphate due to the electrostatic interactions [12]. It is known that the three pK_a values of phosphate are 2.2, 7.2 and 12.4 respectively according to the water chemistry, and phosphate predominantly species existed in anionic forms of HPO_4^{2-} or $H_2PO_4^-$ over the tested pH range. The speciation in solution of the LBR-Zr played an important role in the phosphate adsorption. The main solution species were changed from HPO_4^{2-} to $H_2PO_4^-$ when pH was decreased, and the $H_2PO_4^-$ was rather partial to ligand adsorption [60].

3.7. Effect of coexisting anions

It was known that the real wastewater contained several different kinds of anions that may hinder phosphate adsorption. Thus, the effect of foreign anions on the adsorption capacity containing a range of competing anions (at a concentration of 300 mg L^{-1}) was investigated. Six typical anions were chosen to investigate the competition effects on phosphate adsorption (Fig. 6). It was found that the phosphate adsorption capacity of LBR-Zr was decreased by 8%, 15%, 21%, 20%, 2% and 4% after the addition of coexisting anions Cl^-, SO_4^{2-}, CO_3^{2-}, HCO_3^{2-}, NO_3^- and F^-, respectively. The results exhibited that the incorporation of foreign anions had little effect on phosphate adsorption. It was worth notable that the CO_3^{2-} anion had the largest influence on the phosphate adsorption capacity among the six anions, which could result from both the competitive adsorption of the anions and the increased of pH induced [60]. It was evident that LBR-Zr should not be applied for remediating phosphate from wastewater with high levels of CO_3^{2-} anions, and this finding was in harmony with previous studies [1,30,61].

3.8. Analysis of adsorption mechanism of phosphate on LBR-Zr

It was worth pointing that, according to the literatures reported by Biswas et al. [1,31], the adsorption mechanism of phosphate on metal based biosorbents were maybe ligand exchange, which happened between phosphate ions and OH^- ions in the solution. To better understand adsorption mechanism of phosphate on LBR-Zr, the structure of raw (LBR-Zr) and treated adsorbents (LBR-Zr-P) were studied using various methods such as SEM-EDX, FTIR, and XPS technologies.

3.8.1. SEM-EDX analysis

The investigations of surface morphology of LBR, LBR-Zr and LBR-Zr-P were performed by SEM. The results are shown in Fig. 7. It was found that a lot of anomaly pores could be observed in the surface of the LBR-Zr (Fig. 7b), suggesting that LBR-Zr had higher specific surface area confirmed by the BET results, which was in favor of large adsorption capacity. It was also obviously observed that average pore size became smaller after adsorption in Fig. 7c, and meanwhile a number of thin lamellas formed a stacking structure decreased the size of the intra-particle voids [56]. This indicated that phosphate was adsorbed onto the surface of LBR-Zr and formed a layer of phosphate substance [62,63]. Fig. 8a–c shows the energy dispersive X-ray (EDX) analysis spectrum of LBR, LBR-Zr and LBR-Zr-P. In comparison with LBR-Zr, there were obvious contents of Zr(IV) in the EDX spectrum of LBR-Zr and phosphate in that of LBR-Zr after adsorption.

3.8.2. FTIR spectra analysis

To demonstrate the accomplishment of phosphate adsorbed on LBR-Zr, the FTIR spectra of LBR-Zr before and after phosphate adsorption (LBR-Zr-P) were studied and presented in Fig. 9. In the FTIR spectrum of LBR-Zr-P, it could be seen that the peak at 965 cm^{-1} assigned to LBR-Zr-OH bands disappeared completely after adsorption compared with LBR-Zr. In addition, there was a broad peak located at 3417 cm^{-1}, which could be attributed to the adsorbed water molecule and the surface hydroxyl groups of LBR. After the phosphate adsorption, the peak of LBR-Zr-P slightly weakened. These results indicated that the replacement of hydroxyl groups and water molecule occurred during the phosphate adsorption process [64]. Meanwhile, an intensive peak appeared at 1026 cm^{-1} characteristic of the bending vibration of adsorbed $H_2PO_4^-$ in the spectrum of the phosphate absorbed LBR-Zr, indicating that surface hydroxyl groups were replaced by phosphate [58,64]. Besides, two weak shoulder peaks appeared at 1127 cm^{-1}

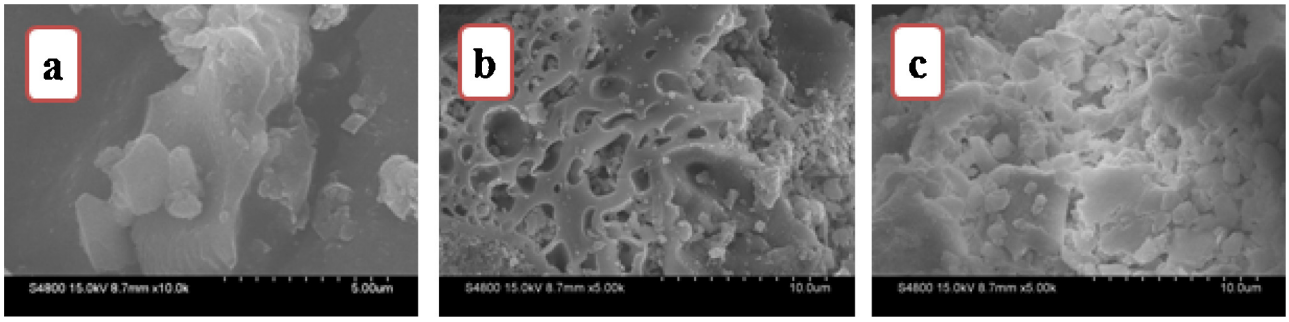

Fig. 7. The SEM images of LBR (a), LBR-Zr before adsorption (b) and LBR-Zr after adsorption (c).

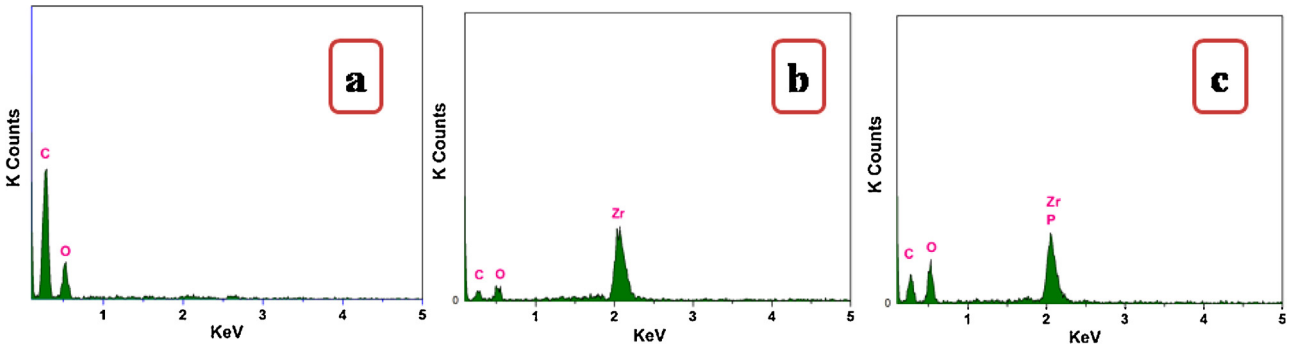

Fig. 8. The EDX of LBR (a), LBR-Zr before adsorption (b) and LBR-Zr after adsorption (c).

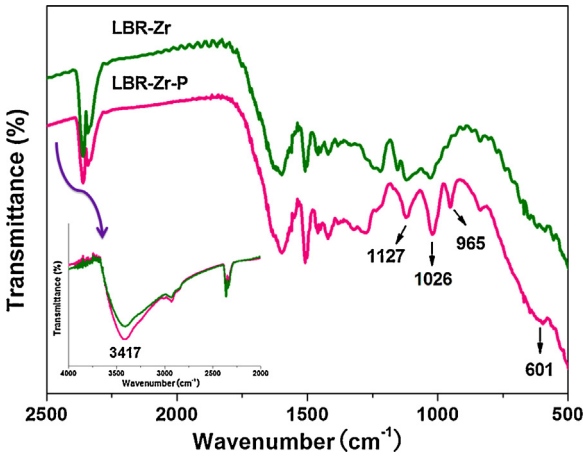

Fig. 9. FTIR spectra of LBR-Zr before and after phosphate adsorption.

and 601 cm^{-1}, which were assigned to the variation of P-O bands [10,24,41]. It was evident that the surface hydroxyl groups of the adsorbent played an important role in the phosphate adsorption process.

3.8.3. XPS spectra analysis

To gain further insights in the phosphate adsorption on LBR-Zr, the XPS of LBR-Zr without and with phosphate adsorption were also analyzed, respectively. From the typical XPS spectra as shown in Fig. 10a, a new peak at the binding energy of approximately 133.6 eV appeared after phosphate loaded on LBR-Zr, corresponding to phosphate group [45]. This provided the evidence of phosphate adsorbed on the surface of the LBR-Zr. Zr3d spectra of the LBR-Zr, before and after adsorption, are displayed in Fig. 10b and c. It was found that chemical environmental of Zr3d changed and shifted to a higher binding energy by about 0.3 eV. That was, hydroxyl groups of LBR-Zr were partially substituted by phosphate anion and the new zirconium species (Zr-O-P) was formed after absorption [62]. A higher electronegativity value of element P (2.19) compared to that of element H (2.1) lead to the lower the negative charge density of Zr in Zr-O-P, which in turn raised binding energy of Zr3d in LBR-Zr after phosphate adsorption. This suggested that phosphate had been chemically adsorbed on the surface of the LBR-Zr [32,33,65,66].

Furthermore, according to the binding energy of different oxygen species, the O 1s XPS spectra of LBR-Zr before and after phosphate adsorption were divided into three peaks, including oxide oxygen (O^{2-}), hydroxyl group (−OH) and adsorbed water (H_2O) [64,67]. It was found that the O 1s spectra and oxygen species percentage of LBR-Zr-P were different from those of LBR-Zr. The percentage of −OH was about 43.74% for LBR-Zr before the phosphate adsorption (Fig. 11a), while Fig. 11b demonstrated that the percentage of −OH reduced to about 25.51% after the phosphate adsorption, which further suggested that hydroxyl groups existed on the surface of LBR-Zr participated in the phosphate adsorption. Thus, the XPS analysis further confirmed that the surface hydroxyl groups played a key role in the phosphate adsorption, which was consistent with the results of above FTIR studies.

Based on the above experimental and technologies analyses, the adsorption mechanism of phosphate on LBR-Zr was proposed as shown in Fig. 12. The phosphate was firstly transferred from aqueous solution to the active sites of the LBR-Zr, and phosphate ions may then further exchange with hydroxyl groups asring from $Zr(OH)_2^{2+}$ species, which caused the release of OH^- to aqueous solution. The formation of proposed adsorption mechanism was further evidenced by monitoring the aqueous solution pH change during the phosphate adsorption process (as shown in Fig. 5 (inserted)). It was clearly found that the final pH value was increased to 4.82 when the initial pH value was 4.02. But the final pH was not changed much. This was maybe because that the content of ZrO_2 load in LBR was low, and meanwhile, the adsorbent dosage was a relatively small amount as well (0.5 g L^{-1}). As a result, the concentration of the release of OH^- to aqueous solution ought to be low

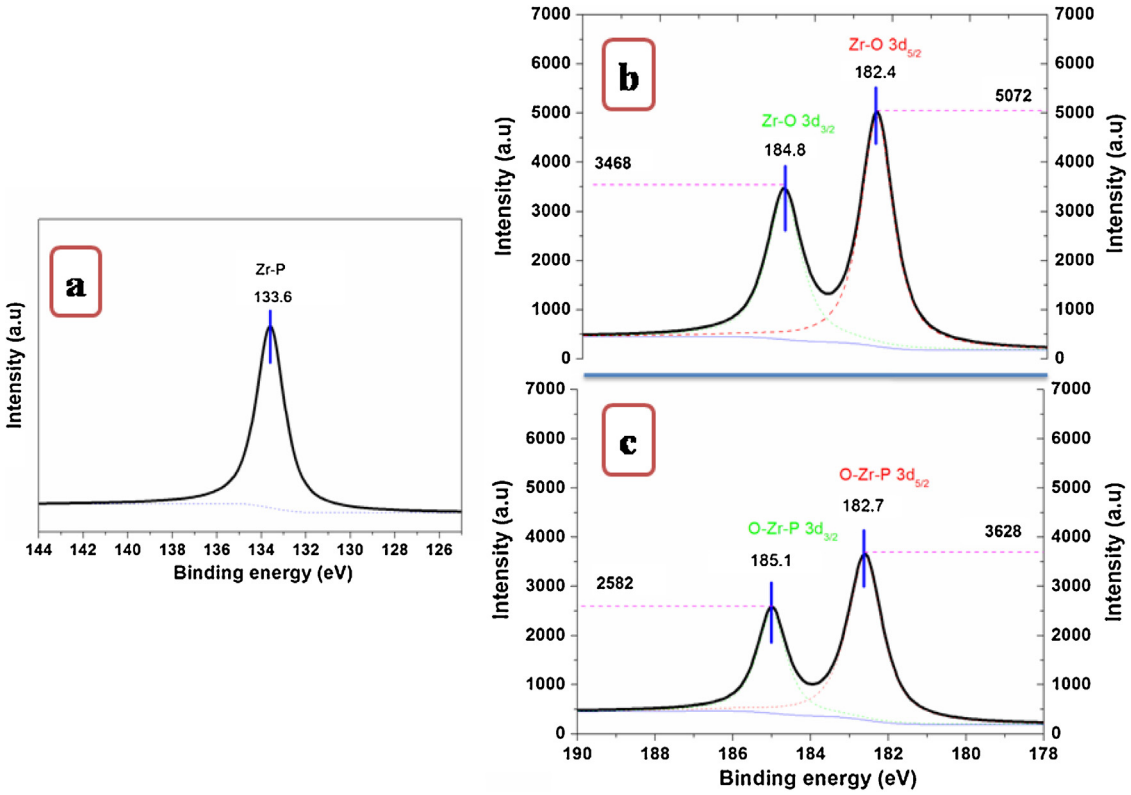

Fig. 10. XPS spectra of P in LBR-Zr-P (a), Zr3d before phosphate adsorption (b) and Zr3d after phosphate adsorption (c).

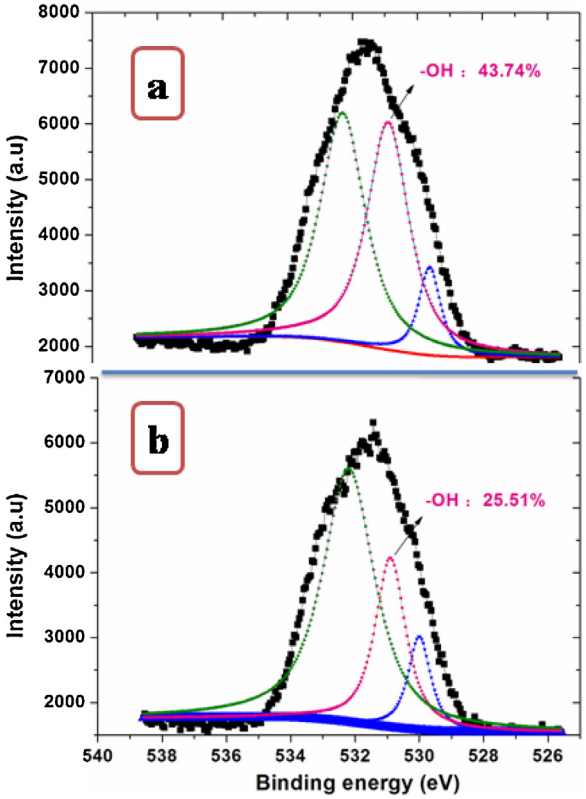

Fig. 11. The surface O 1s spectra of LBR-Zr before (a) and after phosphate adsorption (b).

which could not cause the change of the aqueous solution pH much [24]. Herein, the increase of pH value could be due to the release of

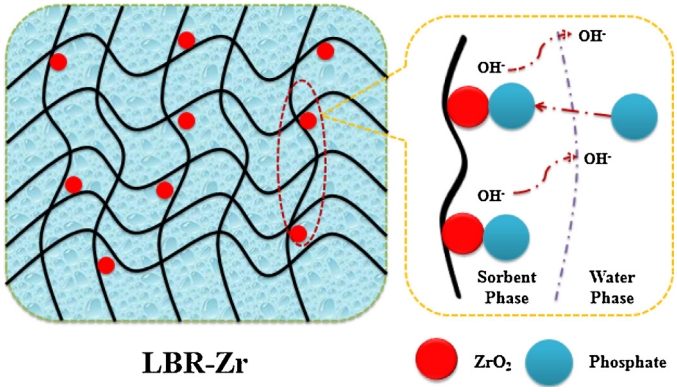

Fig. 12. Possible reactive adsorption mechanism of phosphate ions onto the LBR-Zr.

OH^- when the ligand-exchange reaction between hydroxyl groups asring from adsorbent species and phosphate species occurred. This was a silimar ligand exchange mechanism which had been sepculated in some other literatures [68,69]. In additional, FTIR and XPS analysis confirmed that the surface hydroxyl groups were replaced by the adsorbed phosphate. Therefore, it could be speculated that the main mechanisms of phosphate adsorption on LBR-Zr should be controlled by ligand exchange (chemic sorption).

4. Conclusions

In this present study, a novel LBR-Zr biosorbent was prepared by the post-grafting method followed by ZrO_2 functionalization, which has been proved to be promising for the removal of phosphate. Characterization results confirmed that ZrO_2 was successfully loaded on the surface of LBR via covalence bonding. LBR-Zr exhibited enhanced phosphate adsorption as compared with LBR.

The thermodynamic analysis indicated that phosphate sorption to LBR-Zr increased with increasing temperature from 298 to 338 K, suggesting the spontaneous and endothermic nature of sorption process. Absorption process could be well described by Freundlich and Temkin modes. The kinetic study showed a good compliance with the pseudo-second-order equation. The phosphate removal decreased remarkably as the solution pH increased. Coexisting anions study exhibited that the incorporation of CO_3^{2-} anion had the largest influence on the phosphate adsorption capacity among the six anions (Cl^-, $SO4^{2-}$, CO_3^{2-}, HCO_3^{2-}, NO_3^-, F^- and CO_3^{2-}). The FTIR and XPS spectra analysis indicated that –OH groups played an important role in the adsorption. The LBR-Zr had a potential to be employed as a biosorbent in removal of phosphate from aqueous solutions. This study could provide a new strategy to develop a novel biosorbent for phosphate elimination based on by-products of the bio-butanol industries (lignocellulosic butanol residue).

Acknowledgements

E.M.Z acknowledges the financial support from the Special Fund for the Ecology Key Disciplines of Zhejiang Province in Taizhou University and the Key Research Foundation of Taizhou University with Grant No. 2014PY027. X.H.L acknowledges the financial support from the Program for key Science and Technology Team of Zhejiang Province with Grant No. 2013TD17 and Scientific Research Foundation of Zhejiang Agriculture & Forestry University with Grant No. 2014FR070. S.Y.F acknowledges the financial support from the Program for Zhejiang Provincial Natural Science Foundation of China under Grant No. LZ16C160001. The authors also thank Dr. Jifu wang for the valuable modification.

References

[1] B.K. Biswas, K. Inoue, K.N. Ghimire, H. Harada, K. Ohto, H. Kawakita, Removal and recovery of phosphorus from water by means of adsorption onto orange waste gel loaded with zirconium, Bioresour. Technol. 99 (2008) 8685–8690.
[2] T.A.H. Nguyen, H.H. Ngo, W.S. Guo, J. Zhang, S. Liang, D.J. Lee, P.D. Nguyen, X.T. Bui, Modification of agricultural waste/by-products for enhanced phosphate removal and recovery: potential and obstacles, Bioresour. Technol. 169 (2014) 750–762.
[3] P.U. Verma, A.R. Purohit, N.J. Patel, Pollution status of Chandlodia Lake located in Ahmedabad Gujarat, Int. J. Eng. Res. Appl. 2 (2012) 1600–1610.
[4] L. Chen, X. Zhao, B. Pan, W. Zhang, M. Hua, L. Lv, W. Zhang, Preferable removal of phosphate from water using hydrous zirconium oxide-based nanocomposite of high stability, J. Hazard. Mater. 284 (2015) 35–42.
[5] R. Penetra, M. Reali, E. Foresti, J. Campos, Post-treatment of effluents from anaerobic reactor treating domestic sewage by dissolved-air flotation, Water Sci. Technol. 40 (1999) 137–143.
[6] L. Ruixia, G. Jinlong, T. Hongxiao, Adsorption of fluoride, phosphate, and arsenate ions on a new type of ion exchange fiber, J. Colloid Interface Sci. 248 (2002) 268–274.
[7] R. Chitrakar, S. Tezuka, A. Sonoda, K. Sakane, K. Ooi, T. Hirotsu, Selective adsorption of phosphate from seawater and wastewater by amorphous zirconium hydroxide, J. Colloid Interface Sci. 297 (2006) 426–433.
[8] E. Eggers, A. Dirkzwager, H. Van der Honing, Full-scale experiences with phosphate crystallization in a Crystalactor®, Water Sci. Technol. 23 (1991) 819–824.
[9] S. Benyoucef, M. Amrani, Adsorption of phosphate ions onto low cost Aleppo pine adsorbent, Desalination 275 (2011) 231–236.
[10] A. Rajeswari, A. Amalraj, A. Pius, Removal of phosphate using chitosan-polymer composites, J. Environ. Chem. Eng. 3 (2015).
[11] R. Mallampati, S. Valiyaveettil, Apple peels—a versatile biomass for water purification? ACS Appl. Mater. Interfaces 5 (2013) 4443–4449.
[12] T.A.H. Nguyen, H.H. Ngo, W.S. Guo, J. Zhang, S. Liang, K.L. Tung, Feasibility of iron loaded 'okara' for biosorption of phosphorous in aqueous solutions, Bioresour. Technol. 150 (2013) 42–49.
[13] T.A.H. Nguyen, H.H. Ngo, W.S. Guo, T.V. Nguyen, J. Zhang, S. Liang, S.S. Chen, N.C. Nguyen, A comparative study on different metal loaded soybean milk by-product 'okara' for biosorption of phosphorus from aqueous solution, Bioresour. Technol. 169 (2014) 291–298.
[14] T.L. Eberhardt, S.-H. Min, J.S. Han, Phosphate removal by refined aspen wood fiber treated with carboxymethyl cellulose and ferrous chloride, Bioresour. Technol. 97 (2006) 2371–2376.
[15] N.Y. Mezenner, A. Bensmaili, Kinetics and thermodynamic study of phosphate adsorption on iron hydroxide-eggshell waste, Chem. Eng. J. 147 (2009) 87–96.
[16] T.L. Eberhardt, S.-H. Min, Biosorbents prepared from wood particles treated with anionic polymer and iron salt: effect of particle size on phosphate adsorption, Bioresour. Technol. 99 (2008) 626–630.
[17] C. Namasivayam, D. Sangeetha, Equilibrium and kinetic studies of adsorption of phosphate onto ZnCl2 activated coir pith carbon, J. Colloid Interface Sci. 280 (2004) 359–365.
[18] W. Zhang, Y. Ma, C. Wang, S. Li, M. Zhang, F. Chu, Preparation and properties of lignin–phenol–formaldehyde resins based on different biorefinery residues of agricultural biomass, Ind. Crops Prod. 43 (2013) 326–333.
[19] Y. Jin, X. Cheng, Z. Zheng, Preparation and characterization of phenol–formaldehyde adhesives modified with enzymatic hydrolysis lignin, Bioresour. Technol. 101 (2010) 2046–2048.
[20] J. Yang, J.-X. Wu, Q.-F. Lü, T.-T. Lin, Facile preparation of lignosulfonate–graphene oxide–polyaniline ternary nanocomposite as an effective adsorbent for Pb(II) ions, ACS Sustain. Chem. Eng. 2 (2014) 1203–1211.
[21] Z.-W. He, L.-H. He, J. Yang, Q.-F.;¨ Lu, Removal and recovery of Au(III) from aqueous solution using a low-cost lignin-based biosorbent, Ind. Eng. Chem. Res. 52 (2013) 4103–4108.
[22] Y. Ge, Z. Li, Y. Kong, Q. Song, K. Wang, Heavy metal ions retention by bi-functionalized lignin: synthesis, applications, and adsorption mechanisms, J. Ind. Eng. Chem. 20 (2014) 4429–4436.
[23] H. Harmita, K.G. Karthikeyan, X. Pan, Copper and cadmium sorption onto kraft and organosolv lignins, Bioresour. Technol. 100 (2009) 6183–6191.
[24] J. Liu, Q. Zhou, J. Chen, L. Zhang, N. Chang, Phosphate adsorption on hydroxyl–iron–lanthanum doped activated carbon fiber, Chem. Eng. J. 215 (2013) 859–867.
[25] X. Liu, J. Wang, S. Li, X. Zhuang, Y. Xu, C. Wang, F. Chu, Preparation and properties of UV-absorbent lignin graft copolymer films from lignocellulosic butanol residue, Ind. Crops Prod. 52 (2014) 633–641.
[26] X. Liu, J. Wang, J. Yu, M. Zhang, C. Wang, Y. Xu, F. Chu, Preparation and characterization of lignin based macromonomer and its copolymers with butyl methacrylate, Int. J. Biol. Macromol. 60 (2013) 309–315.
[27] X. Liu, Y. Xu, J. Yu, S. Li, J. Wang, C. Wang, F. Chu, Integration of lignin and acrylic monomers towards grafted copolymers by free radical polymerization, Int. J. Biol. Macromol. 67 (2014) 483–489.
[28] X. Liu, E. Zong, J. Jiang, S. Fu, J. Wang, B. Xu, W. Li, X. Lin, Y. Xu, C. Wang, Preparation and characterization of lignin-graft-poly(ε-caprolactone) copolymers based on lignocellulosic butanol residue, Int. J. Biol. Macromol. 81 (2015) 521–529.
[29] E. Zong, J. jiang, X. Liu, S. Fu, Y. Xu, F. Chu, Combination of lignin and L-lactide towards grafted copolymers from lignocellulosic butanol residue, Int. J. Biol. Macromol. 86 (2016) 80–88.
[30] J. Yang, L. Zhou, L. Zhao, H. Zhang, J. Yin, G. Wei, K. Qian, Y. Wang, C. Yu, A designed nanoporous material for phosphate removal with high efficiency, J. Mater. Chem. 21 (2011) 2489–2494.
[31] B.K. Biswas, K. Inoue, K.N. Ghimire, S. Ohta, H. Harada, K. Ohto, H. Kawakita, The adsorption of phosphate from an aquatic environment using metal-loaded orange waste, J. Colloid Interface Sci. 312 (2007) 214–223.
[32] E. Zong, D. Wei, H. Wan, S. Zheng, Z. Xu, D. Zhu, Adsorptive removal of phosphate ions from aqueous solution using zirconia-functionalized graphite oxide, Chem. Eng. J. 221 (2013) 193–203.
[33] Y. Tang, E. Zong, H. Wan, Z. Xu, S. Zheng, D. Zhu, Zirconia functionalized SBA-15 as effective adsorbent for phosphate removal, Microporous Mesoporous Mater. 155 (2012) 192–200.
[34] J. Zhang, Z. Ma, J. Jiao, H. Yin, W. Yan, E.W. Hagaman, J. Yu, S. Dai, Surface functionalization of mesoporous silica SBA-15 by liquid-phase grafting of zirconium phosphate, Microporous Mesoporous Mater. 129 (2010) 200–209.
[35] K.K. Shah, J. Saikia, D. Saikia, A.K. Talukdar, Synthesis and characterization of isomorphously zirconium substituted mobil five (MFI) zeolite, Mater. Chem. Phys. 134 (2012) 43–49.
[36] B. Rakshe, V. Ramaswamy, S.G. Hegde, R. Vetrivel, A.V. Ramaswamy, Crystalline, microporous zirconium silicates with MFI structure, Catal. Lett. 45 (1997) 41–50.
[37] U.B. Saxena, A.K. Rai, V.K. Mathur, R.C. Mehrotra, D. Radford, Reactions of zirconium isopropoxide with [small beta]-diketones and [small beta]-keto-esters, J. Chem. Soc. A: Inorg. Phys. Theor. (1970) 904–907.
[38] Y. Shan, L. Gao, Synthesis and characterization of phase controllable ZrO2-carbon nanotube nanocomposites, Nanotechnology 16 (2005) 625–630.
[39] Y.-M. Zheng, S.-F. Lim, J.P. Chen, Preparation and characterization of zirconium-based magnetic sorbent for arsenate removal, J. Colloid Interface Sci. 338 (2009) 22–29.
[40] B.L. Kirsch, S.H. Tolbert, Stabilization of isolated hydrous amorphous and tetragonal zirconia nanoparticles through the formation of a passivating alumina shell, Adv. Funct. Mater. 13 (2003) 281–288.
[41] Q. Zhang, Q. Du, T. Jiao, B. Pan, Z. Zhang, Q. Sun, S. Wang, T. Wang, F. Gao, Selective removal of phosphate in waters using a novel of cation adsorbent: zirconium phosphate (ZrP) behavior and mechanism, Chem. Eng. J. 221 (2013) 315–321.
[42] R. Rostamian, M. Najafi, A.A. Rafati, Synthesis and characterization of thiol-functionalized silica nano hollow sphere as a novel adsorbent for removal of poisonous heavy metal ions from water: kinetics, isotherms and error analysis, Chem. Eng. J. 171 (2011) 1004–1011.
[43] B. Kostura, H. Kulveitova, J. Lesko, Blast furnace slags as sorbents of phosphate from water solutions, Water Res. 39 (2005) 1795–1802.

[44] E.A. Deliyanni, E.N. Peleka, N.K. Lazaridis, Comparative study of phosphates removal from aqueous solutions by nanocrystalline akaganeite and hybrid surfactant-akaganeite, Sep. Purif. Technol. 52 (2007) 478–486.
[45] J. Lǔ, H. Liu, R. Liu, X. Zhao, L. Sun, J. Qu, Adsorptive removal of phosphate by a nanostructured Fe–Al–Mn trimetal oxide adsorbent, Powder Technol. 233 (2013) 146–154.
[46] S. Wang, X. Jin, H. Zhao, F. Wu, Phosphate biosorption characteristics of a submerged macrophyte Hydrilla verticillata, Aquat. Bot. 89 (2008) 23–26.
[47] X. Xu, B. Gao, Q. Yue, Q. Zhong, Sorption of phosphate onto giant reed based adsorbent: FTIR, Raman spectrum analysis and dynamic sorption/desorption properties in filter bed, Bioresour. Technol. 102 (2011) 5278–5282.
[48] J. Zhang, W. Shan, J. Ge, Z. Shen, Y. Lei, W. Wang, Kinetic and equilibrium sudies of liquid-phase adsorption of phosphate on modified sugarcane bagasse, J. Environ. ENG. 138 (2011) 252–258.
[49] K. Riahi, B.B. Thayer, A.B. Mammou, A.B. Ammar, M.H. Jaafoura, Biosorption characteristics of phosphates from aqueous solution onto Phoenix dactylifera L. date palm fibers, J. Hazard. Mater. 170 (2009) 511–519.
[50] S.-Y. Yoon, C.-G. Lee, J.-A. Park, J.-H. Kim, S.-B. Kim, S.-H. Lee, J.-W. Choi, Kinetic, equilibrium and thermodynamic studies for phosphate adsorption to magnetic iron oxide nanoparticles, Chem. Eng. J. 236 (2014) 341–347.
[51] M. Arshadi, S. Foroughifard, J.E. Gholtash, A. Abbaspourrad, Preparation of iron nanoparticles-loaded Spondias purpurea seed waste as an excellent adsorbent for removal of phosphate from synthetic and natural waters, J. Colloid Interface Sci. 452 (2015) 69–77.
[52] A.S. Saini, J.S. Melo, Biosorption of uranium by melanin: kinetic, equilibrium and thermodynamic studies, Bioresour. Technol. 149 (2013) 155–162.
[53] Z. Aksu, Determination of the equilibrium, kinetic and thermodynamic parameters of the batch biosorption of nickel(II) ions onto Chlorella vulgaris, Process Biochem. 38 (2002) 89–99.
[54] Y.-S. Ho, G. McKay, Pseudo-second order model for sorption processes, Process Biochem. 34 (1999) 451–465.
[55] H. Trivedi, V. Patel, R. Patel, Adsorption of cellulose triacetate on calcium silicate, Eur. Polym. J. 9 (1973) 525–531.
[56] L.-g. Yan, Y.-y. Xu, H.-q. Yu, X.-d. Xin, Q. Wei, B. Du, Adsorption of phosphate from aqueous solution by hydroxy-aluminum, hydroxy-iron and hydroxy-iron–aluminum pillared bentonites, J. Hazard. Mater. 179 (2010) 244–250.
[57] K.V. Kumar, K. Porkodi, Modelling the solid–liquid adsorption processes using artificial neural networks trained by pseudo second order kinetics, Chem. Eng. J. 148 (2009) 20–25.
[58] M.-L. Chen, C.-B. Huo, Y.-K. Li, J.-H. Wang, Selective adsorption and efficient removal of phosphate from aqueous medium with graphene-lanthanum composite, ACS Sustain. Chem. Eng. 4 (2016) 1296–1302.
[59] L. Zhang, Q. Zhou, J. Liu, N. Chang, L. Wan, J. Chen, Phosphate adsorption on lanthanum hydroxide-doped activated carbon fiber, Chem. Eng. J. 185–186 (2012) 160–167.
[60] Z. Wang, M. Xing, W. Fang, D. Wu, One-step synthesis of magnetite core/zirconia shell nanocomposite for high efficiency removal of phosphate from water, Appl. Surf. Sci. 366 (2016) 67–77.
[61] Q. Liu, P. Hu, J. Wang, L. Zhang, R. Huang, Phosphate adsorption from aqueous solutions by zirconium(IV) loaded cross-linked chitosan particles, J. Taiwan Inst. Chem. Eng. 59 (2016) 311–319.
[62] J. Wang, X. Lin, X. Luo, Y. Long, A sorbent of carboxymethyl cellulose loaded with zirconium for the removal of fluoride from aqueous solution, Chem. Eng. J. 252 (2014) 415–422.
[63] X.-j. Hu, J.-s. Wang, Y.-g. Liu, X. Li, G.-m. Zeng, Z.-l. Bao, X.-x. Zeng, A.-w. Chen, F. Long, Adsorption of chromium(VI) by ethylenediamine-modified cross-linked magnetic chitosan resin: isotherms, kinetics and thermodynamics, J. Hazard. Mater. 185 (2011) 306–314.
[64] Y. Su, H. Cui, Q. Li, S. Gao, J.K. Shang, Strong adsorption of phosphate by amorphous zirconium oxide nanoparticles, Water Res. 47 (2013) 5018–5026.
[65] W. Wang, J. Zhou, D. Wei, H. Wan, S. Zheng, Z. Xu, D. Zhu, ZrO2-functionalized magnetic mesoporous SiO2 as effective phosphate adsorbent, J. Colloid Interface Sci. 407 (2013) 442–449.
[66] W. Wang, H. Zhang, L. Zhang, H. Wan, S. Zheng, Z. Xu, Adsorptive removal of phosphate by magnetic Fe3O4@C@ZrO2, Colloids Surf. A: Physicochem. Eng. Aspects 469 (2015) 100–106.
[67] Y. Zhang, M. Yang, X.-M. Dou, H. He, D.-S. Wang, Arsenate adsorption on an Fe–Ce bimetal oxide adsorbent: role of surface properties, Environ. Sci. Technol. 39 (2005) 7246–7253.
[68] W.-Y. Huang, D. Li, Z.-Q. Liu, Q. Tao, Y. Zhu, J. Yang, Y.-M. Zhang, Kinetics, isotherm, thermodynamic, and adsorption mechanism studies of La (OH) 3-modified exfoliated vermiculites as highly efficient phosphate adsorbents, Chem. Eng. J. 236 (2014) 191–201.
[69] N. Chen, C. Feng, Z. Zhang, R. Liu, Y. Gao, M. Li, N. Sugiura, Preparation and characterization of lanthanum(III) loaded granular ceramic for phosphorus adsorption from aqueous solution, J. Taiwan Inst. Chem. Eng. 43 (2012) 783–789.